

A Robust Extended H_∞ Filtering Approach to Multi-Robot Cooperative Localization in Dynamic Indoor Environments

Yan Zhuang, Zidong Wang, Haiyang Yu, Wei Wang and Stanislaw Lauria

Abstract

Multi-robot cooperative localization serves as an essential task for a team of mobile robots to work within an unknown environment. Based on the real-time laser scanning data interaction, a robust approach is proposed to obtain optimal multi-robot relative observations by using the Metric-based Iterative Closest Point (MbICP) algorithm, which makes it possible to utilize the surrounding environment information directly instead of placing a localization-mark on the robots. To meet the demand of dealing with the inherent nonlinearities existing in the multi-robot kinematic models and the relative observations, a robust extended H_∞ filtering (REHF) approach is developed for the multi-robot cooperative localization system, which could handle non-Gaussian process and measurement noises with respect to robot navigation in unknown dynamic scenes. Compared with the conventional multi-robot localization system using extended Kalman filtering (EKF) approach, the proposed filtering algorithm is capable of providing superior performance in a dynamic indoor environment with outlier disturbances. Both numerical experiments and experiments conducted for the Pioneer 3-DX robots show that the proposed localization scheme is effective in improving both the accuracy and reliability of the performance within a complex environment.

Keywords

Multi-robot cooperative localization; robust extended H_∞ filtering (REHF); metric-based iterative closest point (MbICP); laser data interaction.

I. INTRODUCTION

With the fast development of mobile robotics and advanced techniques in practical applications, single robot is usually unable to fulfil more and more sophisticated tasks in a large-scale dynamic environment. In recent years, cooperative robotics has emerged as a new research branch that focuses on the problem of coordinating teams of mobile robots, such as multi-robot exploration and coordination of robotic networks in *Rooker and Birk (2007)* and *Nowzari and Cortes (2012)*. In particular, the multi-robot cooperative localization problem

This work was supported in part by the National Natural Science Foundation of China under grants 61075094, 61035005 and 61134009.

Y. Zhuang, H. Yu and W. Wang are with the Research Center of Information and Control, Dalian University of Technology, Dalian 116024, China.

Z. Wang and S. Lauria are with the Department of Information Systems and Computing, Brunel University, Uxbridge, Middlesex, UB8 3PH, United Kingdom.

All correspondences concerning this paper should be addressed to Zidong Wang. (Email: Zidong.Wang@brunel.ac.uk)

is fundamental to cooperative robotics. In a multi-robot cooperative localization system, each robot's position and orientation would need to be estimated effectively in the composite state space by using information sensing of the environment and communication between different robots, which gives rise to significant challenges and complexities (Fox, Burgard, Kruppa, & Thrun 2000 and Mourikis & Roumeliotis 2006b).

Recently, a variety of approaches have been developed for multi-robot cooperative localization. In the case that only the robots themselves are considered as landmarks, a method using a combination of maximum likelihood estimation and numerical optimization was proposed for localizing the members of a mobile robot team in Howard, Mataric, and Sukhatme (2002). As reported in some multi-robot cooperative localization systems, a group of robots were divided into several teams and only one team was moving while all the other teams were taken as landmarks for cooperative localization in Rekleitis, Dudek, and Miliotis (2002). Among others, the extended Kalman filter (EKF) has proven to be most popular for multi-robot localization problems in the case that the process and measurement noises are of the Gaussian type. A centralized extended Kalman filtering method for multi-robot localization was analyzed in Kondaxakis, Ruiz, and Harwin (2004), where detailed localization equations were derived in a matrix expression. By writing the equations for centralized estimator in a decentralized form, the single Kalman filter was allowed to be decomposed into a number of smaller communicating filters. A distributed extended Kalman filtering method for multi-robot localization was proposed in Roumeliotis and Bekey (2002), where the uncertainty of robot pose and the update process for robot position estimation were discussed in detail. In order to exploit the information contained in any relative observation between two robots, a generic relative observation was integrated into EKF equations to accomplish cooperative localization in Martinelli, Pont, and Siegwart (2005). Some alternative approaches were also used in the robotics literature, for example, Fox, Burgard, Kruppa, and Thrun (2000) proposed a statistical algorithm for multi-robot cooperative localization by using the sample-based version of Markov localization, where the probability distribution updating through relative observations was used to describe robots' positioning accuracy.

In this paper, a new approach based on real-time laser data interaction and robust extended H_∞ filtering (REHF) is presented to solve multi-robot cooperative localization problem in dynamic indoor scenes. The new relative observation technique between any two robots without placing a special localization-mark on the robots stems from the actual needs in our work. Generally speaking, mobile robots should be large enough so that they can detect each other effectively. As introduced in Huang, Farritor, Qadi, and Goddard (2006), the robot platform was approximately 130-cm high and 50-cm diameter, and a SICK laser scanner LMS200 mounted on the robot was used to estimate the relative position between two robots. However, if only a middle-sized robot (eg. Pioneer3-DX) is available, a special localization-mark is often placed in the top of mobile robot platform and the robot should carry it in the course of localization (Mourikis & Roumeliotis 2006a), which would increase the robot's load and make it inconvenient in some applications. In addition, a vision system installed on the ceiling of laboratory was used to obtain relative observations in Mourikis

and Roumeliotis (2006b). Unfortunately, such a system is expensive and the experimental scene should be structured and customized. In Chen, Sun, Yang, and Chen (2010), a ceiling vision-based localization approach was used to perform the global localization, but the validity of its feature detection algorithm had to depend on the regular pattern in a clear ceiling. There have been also many successful applications of multi-robot localization in robot soccer, but the working environment of multiple soccer robots is required to be completely structured and pre-arranged. To provide accurate relative observations even when there are dynamic obstacles in the environment, an alternative cooperative measurement approach is designed without adding any other equipments in the multi-robot cooperative localization system. By using a Metric-based Iterative Closest Point (MbICP) algorithm proposed in Minguez, Montesano, and Lamiraux (2006) to perform 2D laser data matching, an optimal relative observations (relative distance and orientation) can be derived between any two robots equipped with laser range finders. The advantage of the MbICP-based measurement approach lies in that it could use the information obtained from the surrounding environment instead of the direct measurement from a special localization-mark used in the traditional methods.

How to make a multi-robot cooperative localization system capable of adapting the unknown dynamic environment is another problem stemming from the real applications. The mainstream approach for mobile robot localization is Bayesian estimation. When the process and measurement error are assumed Gaussian, the Bayesian approach results in the classical extended Kalman filtering (EKF) framework. However, EKF is not designed to solve outlier disturbance such as unexpected collisions and wheel-slippage, which are all the typical non-Gaussian noises in the multi-robot cooperative localization system. Therefore, an alternative filtering algorithm to the conventional EKF approach should be proposed to estimate each robot's pose in this work. To handle this problem, the REHF algorithm is used in this paper to implement multi-robot cooperative localization, which could deal with the nonlinear kinematic models of the multi-robot systems, the nonlinear relative distance and orientation measurement, as well as the non-Gaussian noises resulted from the unexpected collisions with passersby (or other dynamic obstacles) while service robot is navigating in unknown indoor environment (such as hospitals and offices). The superior performances of multi-robot cooperative localization based on laser data interaction and REHF are confirmed through experimental results.

The remainder of this paper is organized as follows. Section II shows the kinematics of the multi-robot system and the relative observations. Section III presents multi-robot relative observation approach based on MbICP algorithm. The design of multi-robot cooperative localization system using the REHF algorithm is introduced in Section IV. Section V gives the results of numerical experiments and the experiment implemented on two Pioneer 3-DX mobile robots, which demonstrate the effectiveness of the proposed design method. Concluding remarks and future work are given in Section VI.

Notation The notation $X \geq Y$ (respectively, $X > Y$) where X and Y are symmetric matrices, means that $X - Y$ is positive semi-definite (respectively, positive definite). The superscript T stands for matrix transposition. $\|f_k\|_R^2$ means the product $f_k^T R f_k$. Gramian matrix is denoted by $R_x = \langle x, x \rangle$, where x is a

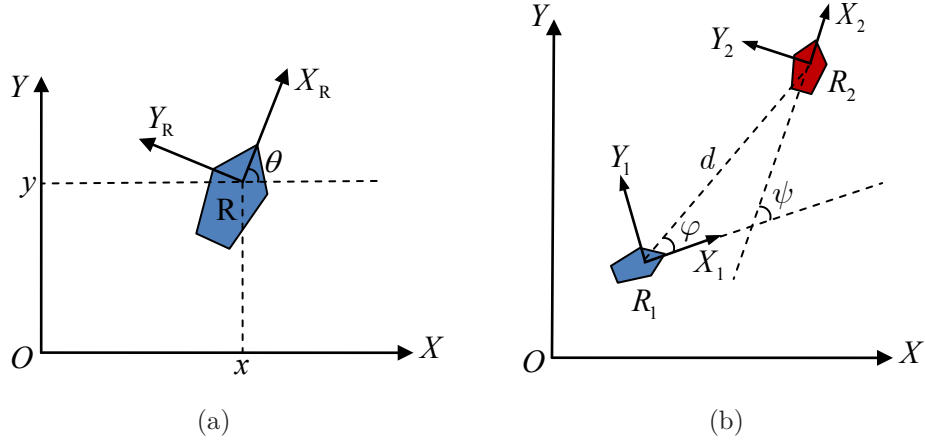


Fig. 1. (a) Position and orientation of robot R_i in global coordinate system; (b) Relative observation between two robots.

vector and $\langle x, x \rangle$ stands for the inner product of x , i.e. $\langle x, x \rangle = xx^T$.

II. KINEMATICS MODEL AND RELATIVE OBSERVATION

Let XOY be the global coordinate system and the pose of robot R_i in XOY be $z_i = [x_i, y_i, \theta_i]^T$ as shown in Fig. 1(a) where x_i and y_i are the coordinates of robot R_i on X -axis and Y -axis, respectively, and θ_i is the angle between X -direction and X_R -direction. $u_i = [v_i, \omega_i]^T$ is the estimate of input for R_i using odometer, where v_i and ω_i are, respectively, the estimates of linear velocity input and angular velocity input for R_i . $\xi_{i,k} = [\xi_{x_i,k}, \xi_{y_i,k}, \xi_{\theta_i,k}]^T$ is the state error. Then, the multi-robot system formed by R_1 and R_2 can be described by the following equations:

$$\begin{cases} x_{i,k+1} = x_{i,k} + \Delta T v_{i,k} \cos \theta_{i,k} + \xi_{x_{i,k}} \\ y_{i,k+1} = y_{i,k} + \Delta T v_{i,k} \sin \theta_{i,k} + \xi_{y_{i,k}} \\ \theta_{i,k+1} = \theta_{i,k} + \Delta T \omega_{i,k} + \xi_{\theta_{i,k}} \end{cases} \quad i = 1, 2. \quad (1)$$

Denoting $z_k = \begin{bmatrix} z_{1,k} \\ z_{2,k} \end{bmatrix}$, $u_k = \begin{bmatrix} u_{1,k} \\ u_{2,k} \end{bmatrix}$, $\xi_k = \begin{bmatrix} \xi_{1,k} \\ \xi_{2,k} \end{bmatrix}$ and $k \in [0, N]$, (1) can be rewritten as

$$z_{k+1} = f(z_k, u_k, \xi_k), \quad (2)$$

where

$$f(z_k, u_k, \xi_k) = \begin{bmatrix} x_{1,k} \\ y_{1,k} \\ \theta_{1,k} \\ x_{2,k} \\ y_{2,k} \\ \theta_{2,k} \end{bmatrix} + \Delta T \begin{bmatrix} v_{1,k} \cos \theta_{1,k} \\ v_{1,k} \sin \theta_{1,k} \\ \omega_{1,k} \\ v_{2,k} \cos \theta_{2,k} \\ v_{2,k} \sin \theta_{2,k} \\ \omega_{2,k} \end{bmatrix} + \begin{bmatrix} \xi_{x_{1,k}} \\ \xi_{y_{1,k}} \\ \xi_{\theta_{1,k}} \\ \xi_{x_{2,k}} \\ \xi_{y_{2,k}} \\ \xi_{\theta_{2,k}} \end{bmatrix}. \quad (3)$$

For the single robot localization, a localization-mark is usually used, then the distance and angle between the robot and the mark are treated as the observation, which is an absolute measurement. Here, for the multi-robot localization, the robots observe each other and treat the relative observation as the measurement (see Fig. 1(b)).

Denote d, φ, ψ as the measurement of robot R_1 to R_2 , where

$$d = \sqrt{(x_2 - x_1)^2 + (y_2 - y_1)^2} \quad (4)$$

is the distance between R_1 and R_2 ,

$$\varphi = \arctan \frac{-(x_2 - x_1) \sin \theta_1 + (y_2 - y_1) \cos \theta_1}{(x_2 - x_1) \cos \theta_1 + (y_2 - y_1) \sin \theta_1} \quad (5)$$

is the azimuth of R_2 relative to X_1 -direction, and

$$\psi = \theta_2 - \theta_1 \quad (6)$$

is the angle between X_1 -direction and X_2 -direction. Supposing $\eta_k = [\eta_{d,k}, \eta_{\varphi,k}, \eta_{\psi,k}]^T$ is the measurement errors at moment k , (4)-(6) can be rewritten in a compact form as $m_k = g(z_k, \eta_k)$ where

$$g(z_k, \eta_k) = \begin{bmatrix} d_k + \eta_{d,k} \\ \varphi_k + \eta_{\varphi,k} \\ \psi_k + \eta_{\psi,k} \end{bmatrix}. \quad (7)$$

To this end, the system state equation and measurement equation for the multi-robot system have been obtained and expressed as follows:

$$\begin{aligned} z_{k+1} &= f(z_k, u_k, \xi_k), \\ m_k &= g(z_k, \eta_k). \end{aligned}$$

In an ideal situation, the nature of the process and observation errors could be assumed to be Gaussian white noises (for example, in a typical extended Kalman filtering approach). However, in many robotics applications, these assumptions are unpractical and may seriously degrade the localization accuracy. In fact, the distribution of the sensor and process noise is generally multi-modal and imprecisely known in the multi-robot cooperative localization task in this work, especially when the unexpected collisions with passersby or other dynamic obstacles were happened while a robot is navigating in an unknown indoor environment.

III. LASER DATA INTERACTION BASED ON MBICP ALGORITHM

ICP (Iterative Closest Point) algorithm is a straightforward method to align two free-form shapes, which was presented by *Besl and McKay (1992)*. Among many variants of ICP proposed in recent years, MbICP algorithm is a new scan matching technique for mobile robot displacement estimation, which was proposed by *Minguez, Montesano, and Lamiraux (2006)* and is usually used in matching dense two-dimensional range

scans. By using the MbICP algorithm, an optimal analytical solution can be derived for the translation and rotation between two groups of scanning data if the overlapping scanning region is large enough. Compared with classical ICP algorithm, MbICP algorithm uses a new metric distance ($\|q\| := \sqrt{x^2 + y^2 + L^2\theta^2}$, where L is a constant factor) defined in the configuration space of the sensor, which pays more attention to the influencing factor of rotational displacement and can rectify the rotation error more precisely than the ICP algorithm.

In the process of multi-robot cooperative localization, it is necessary to obtain the relative pose between different robots. Each robot in the cooperative localization system is equipped with a laser range finder and wireless network adapter, which can acquire laser scanning data and communicate with each other in real time. While multiple robots are working in the same scene, they can utilize the surrounding environment as the intermediary to obtain the relative pose indirectly through the real-time laser data matching.

Suppose that M_1, M_2 are the laser scanning data sets obtained by robot R_1 and R_2 . MbICP algorithm is applied to accomplish the optimal scanning data matching, and $\tilde{z}_{12} = (\tilde{x}_{12}, \tilde{y}_{12}, \tilde{\theta}_{12})^T$ is obtained and defined as the optimal relative pose. The corresponding error covariance is also calculated simultaneously. The process of a coarse-to-fine laser scanning data registration based on MbICP consists of the following steps:

(1) Denote $M_1 = \{p_1, \dots, p_n\}$, $M_2 = \{q_1, \dots, q_n\}$. Carry out coarse registration by sampling rotation angle from -90° to 90° every 10° . The closest points correspondences $C(M_1, \tilde{M}_{2,j}, \hat{\theta}_{12,j}) = \{(p_i, \hat{q}_{i,j}) \mid p_i \in M_1, \hat{q}_{i,j} \in \tilde{M}_{2,j}, i = 1, \dots, n\}$ is obtained at the j -th sample, where $\tilde{M}_{2,j} = \left\{ \hat{q}_{i,j} \mid \hat{q}_{i,j} = q_i \begin{bmatrix} \cos \hat{\theta}_{12,j} & \sin \hat{\theta}_{12,j} \\ -\sin \hat{\theta}_{12,j} & \cos \hat{\theta}_{12,j} \end{bmatrix}, q_i \in M_2, i = 1, \dots, n, \hat{\theta}_{12,j} = -90^\circ + j \times 10^\circ \right\}$, $j = 0, 1, \dots, 18$.

(2) Find $\bar{j} \in \{0, 1, \dots, 18\}$ that minimizes $E(\hat{\theta}_{12,j}) = \sum_{i=1}^n d(p_i, \hat{q}_{i,j})^2$, then calculate the translation $t = (\hat{x}_{12}, \hat{y}_{12}) = \frac{1}{n} \sum_{i=1}^n p_i - \frac{1}{n} \sum_{i=1}^n \hat{q}_{i,\bar{j}}$ and obtain the pre-estimation relative pose $\hat{z}_{12} = (\hat{x}_{12}, \hat{y}_{12}, \hat{\theta}_{12,\bar{j}})^T$.

(3) Transform the laser data sets M_1 and $\tilde{M}_{2,\bar{j}}$ from laser coordinate system to their own robot coordinate system, then the new laser data set of robot R_2 is transformed to the coordinate system of robot R_1 according to \hat{z}_{12} . Two laser data sets M'_1 and M'_2 are derived after these transformations.

(4) Use MbICP algorithm to match M'_1 and M'_2 , then derive the optimal analytical solution $S = [x'_{12}, y'_{12}, \theta'_{12}]^T$ by several times of iterative calculation. Now, the optimal relative pose \tilde{z}_{12} between robots R_1 and R_2 can be

calculated in terms of the equation $\tilde{z}_{12} = \hat{z}_{12} + \Lambda S$, where $\Lambda = \begin{bmatrix} \cos \hat{\theta}_{12,\bar{j}} & \sin \hat{\theta}_{12,\bar{j}} & 0 \\ -\sin \hat{\theta}_{12,\bar{j}} & \cos \hat{\theta}_{12,\bar{j}} & 0 \\ 0 & 0 & 1 \end{bmatrix}$.

A series of experiments of laser scanning data matching based on MbICP have been performed with the SICK LMS 200 on Pioneer3-DX, the field of view is 180° in front of the robot and up to $8m$ distance. In order to perform effective and accurate laser scanning data matching in actual experiment, two robots should navigate in the same direction so that there is enough overlapping area between two robot's laser scanning

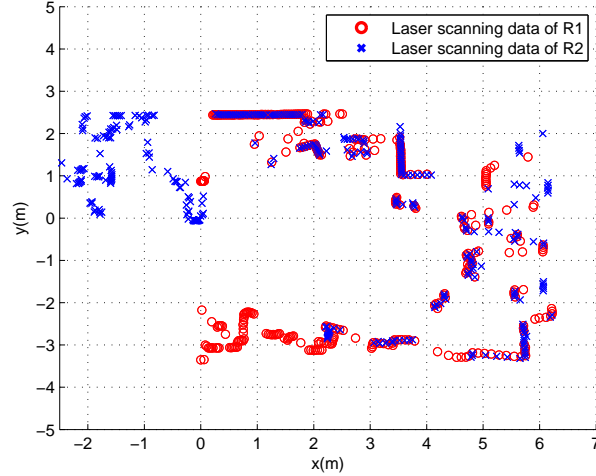


Fig. 2. An optimal matching result \tilde{z}_{12} is obtained by using MbICP algorithm.

fields. The results of multi-robot laser scanning data matching based on MbICP are shown in Fig. 2.

IV. A ROBUST EXTENDED H_∞ FILTER DESIGN

Since $f(z_k, u_k, \xi_k)$ and $g(z_k, \eta_k)$ are nonlinear functions and $\hat{z}_k = \begin{bmatrix} \hat{z}_{1,k} \\ \hat{z}_{2,k} \end{bmatrix}$ is supposed to be the filtered estimates of z_k at moment k , $f(z_k, u_k, \xi_k)$ and $g(z_k, \eta_k)$ can be extended in a Taylor series around $(\hat{z}_k, u_k, 0)$ and $(\hat{z}_k, 0)$ as follows:

$$f(z_k, u_k, \xi_k) = f(\hat{z}_k, u_k, 0) + A_k(z_k - \hat{z}_k) + W_k \xi_k + \sigma_1, \quad (8)$$

$$g(z_k, \eta_k) = g(\hat{z}_k, 0) + C_k(z_k - \hat{z}_k) + V_k \eta_k + \sigma_2, \quad (9)$$

where

$$W_k = \left. \frac{\partial f}{\partial \xi_k} \right|_{z_k=\hat{z}_k, \xi_k=0} = I_6, \quad V_k = \left. \frac{\partial g}{\partial \eta_k} \right|_{z_k=\hat{z}_k, \eta_k=0} = I_6,$$

and the matrices A_k and C_k are given in equations (10) and (11), respectively. σ_1 and σ_2 represent the higher terms of the Taylor series expansions.

Rearrange (8) and (9) as follows:

$$z_{k+1} = A_k z_k + \bar{\xi}_k, \quad (12)$$

$$m_k = C_k z_k + \bar{\eta}_k, \quad (13)$$

where $\bar{\xi}_k = \xi_k + f(\hat{z}_k, u_k, 0) - A_k \hat{z}_k + \sigma_1$, $\bar{\eta}_k = \eta_k + g(\hat{z}_k, 0) - C_k \hat{z}_k + \sigma_2$. The random entries $\bar{\xi}_k$ and $\bar{\eta}_k$ are considered to be the generalized noises which contain the process noise or measurement noise and the nonlinear higher terms of the Taylor series expansions, so they are non-Gaussian type noises generally. In other words, the nonlinear higher terms of the Taylor series expansions have been treated as a non-Gaussian disturbance, which gives one of our motivations to think about the robust extended H_∞ filtering approach.

$$A_k = \frac{\partial f}{\partial z_k} \Big|_{z_k=\hat{z}_k, \xi_k=0} = \begin{bmatrix} 1 & 0 & -\Delta T v_{1,k} \sin \theta_{1,k} & 0 & 0 & 0 \\ 0 & 1 & \Delta T v_{1,k} \cos \theta_{1,k} & 0 & 0 & 0 \\ 0 & 0 & 1 & 0 & 0 & 0 \\ 0 & 0 & 0 & 1 & 0 & -\Delta T v_{2,k} \sin \theta_{2,k} \\ 0 & 0 & 0 & 0 & 1 & \Delta T v_{2,k} \cos \theta_{2,k} \\ 0 & 0 & 0 & 0 & 0 & 1 \end{bmatrix} \Big|_{z_k=\hat{z}_k, \xi_k=0}, \quad (10)$$

$$C_k = \begin{bmatrix} C_{1,k} & C_{2,k} \end{bmatrix}, \quad (11)$$

where

$$C_{1,k} = \frac{\partial g}{\partial z_{1,k}} \Big|_{z_k=\hat{z}_k, \eta_k=0} = \begin{bmatrix} \frac{x_{1,k}-x_{2,k}}{\sqrt{(x_{1,k}-x_{2,k})^2+(y_{1,k}-y_{2,k})^2}} & \frac{y_{1,k}-y_{2,k}}{\sqrt{(x_{1,k}-x_{2,k})^2+(y_{1,k}-y_{2,k})^2}} & 0 \\ \frac{-(y_{1,k}-y_{2,k})}{(x_{1,k}-x_{2,k})^2+(y_{1,k}-y_{2,k})^2} & \frac{x_{1,k}-x_{2,k}}{(x_{1,k}-x_{2,k})^2+(y_{1,k}-y_{2,k})^2} & -1 \\ 0 & 0 & -1 \end{bmatrix} \Big|_{z_k=\hat{z}_k, \eta_k=0},$$

$$C_{2,k} = \frac{\partial g}{\partial z_{2,k}} \Big|_{z_k=\hat{z}_k, \eta_k=0} = \begin{bmatrix} \frac{x_{2,k}-x_{1,k}}{\sqrt{(x_{2,k}-x_{1,k})^2+(y_{2,k}-y_{1,k})^2}} & \frac{y_{2,k}-y_{1,k}}{\sqrt{(x_{2,k}-x_{1,k})^2+(y_{2,k}-y_{1,k})^2}} & 0 \\ \frac{-(y_{2,k}-y_{1,k})}{(x_{2,k}-x_{1,k})^2+(y_{2,k}-y_{1,k})^2} & \frac{x_{2,k}-x_{1,k}}{(x_{2,k}-x_{1,k})^2+(y_{2,k}-y_{1,k})^2} & 0 \\ 0 & 0 & 1 \end{bmatrix} \Big|_{z_k=\hat{z}_k, \eta_k=0}.$$

Let us now build the REHF to estimate the state z_k of multi-robot system. The following theorem guarantees the existence of the filter and gives a practical filter design procedure.

Theorem 1: Let a discrete-time system be given by (12) and (13) with the Gramian matrix

$$\left\langle \begin{bmatrix} z_0 \\ \bar{\xi}_j \\ \bar{\eta}_j \end{bmatrix}, \begin{bmatrix} z_0 \\ \bar{\xi}_k \\ \bar{\eta}_k \end{bmatrix} \right\rangle = \begin{bmatrix} P_{0|-1} & 0 & 0 \\ 0 & Q_k \delta_{jk} & 0 \\ 0 & 0 & R_k \delta_{jk} \end{bmatrix}, \quad (14)$$

here δ_{jk} is Kronecker delta. For a given scalar $\gamma > 0$, if the matrix $\begin{bmatrix} A_k & I \end{bmatrix}$ has full rank, then for all nonzero $\bar{\xi}_k$ and $\bar{\eta}_k$, there exists a filter achieving the following performance:

$$\frac{\sum_{k=0}^N \|\tilde{z}_k\|^2}{\|z_0 - z_{0|-1}\|_{P_{0|-1}}^2 + \sum_{k=0}^{N-1} \|\bar{\xi}_k\|_{Q_k}^2 + \sum_{k=0}^N \|\bar{\eta}_k\|_{R_k}^2} < \gamma^2, \quad (15)$$

where $\tilde{z}_k = z_k - \hat{z}_k$, if and only if the filtering error covariance matrix $P_{k|k}$ satisfies

$$P_{k|k}^{-1} = P_{k|k-1}^{-1} + C_k^T R_k^{-1} C_k - \gamma^{-2} I > 0, \quad 0 \leq k \leq N,$$

where the initial values is $P_{0|-1}$, and the predicted error covariance matrix $P_{k|k-1}$ satisfies the Riccati recursion:

$$P_{k|k-1} = A_{k-1} P_{k-1|k-1} A_{k-1}^T + Q_{k-1}. \quad (16)$$

The filtered estimates $\hat{z}_{k|k}$ are recursively computed as

$$\hat{z}_{k|k} = \hat{z}_{k|k-1} + K_k(m_k - C_k \hat{z}_{k|k-1}), \quad (17)$$

where

$$K_k = P_{k|k-1} C_k^T (C_k P_{k|k-1} C_k^T + R_k)^{-1} \quad (18)$$

and the predicted estimates

$$\hat{z}_{k|k-1} = A_{k-1} \hat{z}_{k-1|k-1}. \quad (19)$$

Proof: See the appendix. ■

V. EXPERIMENTAL RESULTS

A. Numerical Experiments

Two criteria are used to evaluate the performance of the filter. Let $Z_{i,k} = [X_{i,k}, Y_{i,k}, \Theta_{i,k}]^T$ be the actual position of robot R_i at moment k . Define

$$E_i := \frac{1}{N} \sum_{k=1}^N \sqrt{(\hat{x}_{i,k} - X_{i,k})^2 + (\hat{y}_{i,k} - Y_{i,k})^2}, \quad i = 1, 2, 3 \quad (20)$$

which means the error mean of filtered estimates of R_i from moment 1 to N , and

$$M_i := \max_{1 \leq k \leq N} \sqrt{(\hat{x}_{i,k} - X_{i,k})^2 + (\hat{y}_{i,k} - Y_{i,k})^2}, \quad i = 1, 2, 3 \quad (21)$$

which stands for the maximum deviation of filtered estimates of R_i from moment 1 to N .

In the following numerical experiment of multi-robot cooperative localization, the velocities of robots are all set to range from 100mm/s to 120mm/s , and the process and the measurement errors are assumed to be white Gaussian sequences with outlier disturbances. $Z_{1,0} = [5, 15, \pi/6]^T$, $Z_{2,0} = [-5, 10, -\pi/2]^T$, $Z_{3,0} = [15, -15, \pi/6]^T$ are set as the initial positions. The simulation results are shown in Table I, Fig. 3 and Fig. 4.

TABLE I
ERROR ACCUMULATION AND MAXIMUM DEVIATION OF EKF AND REHF IN NUMERICAL EXPERIMENTS
(UNIT:METER)

	E_1	E_2	E_3	M_1	M_2	M_3
EKF	0.3502	0.3854	0.3050	0.5777	0.5580	0.4957
REHF	0.2001	0.2984	0.1671	0.4348	0.4740	0.4052

As shown in Fig. 3, the black lines are the actual trajectories, the blue lines are the trajectory estimations using EKF, and the red lines are the trajectory estimations using REHF. The outliers on the process error of robot R_1 , R_2 and R_3 occur from timestep 31 to 33, 101 to 103 and 201 to 203, respectively. The outliers on the measurement error of robot R_1 , R_2 and R_3 occur from timestep 81 to 83, 151 to 153 and 251 to 253,

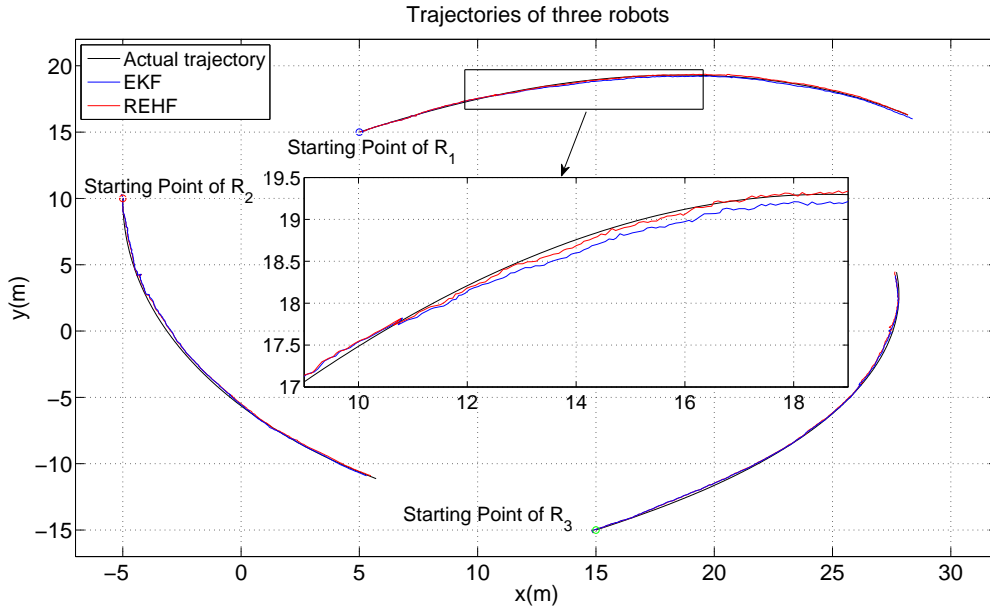


Fig. 3. Three mobile robots' actual trajectories, trajectory estimations using EKF and trajectory estimations using REHF in the numerical experiment.

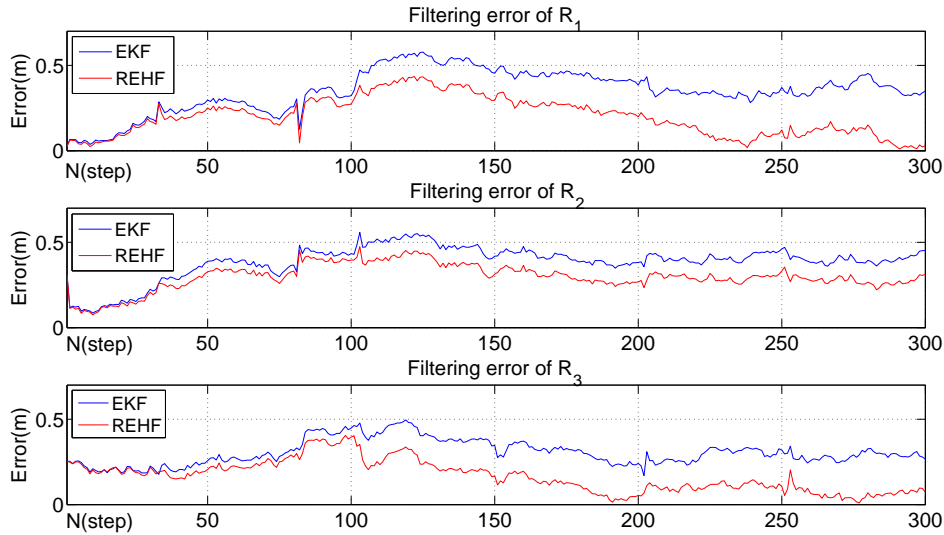


Fig. 4. The position errors of three mobile robots' trajectory estimations, where the blue ones are the filtering errors using EKF and the red ones are the filtering errors using REHF.

respectively. When these outliers happen, the errors of process and measurement are all enlarged for at least more than ten times. The center subfigure in Fig. 3 shows a selection area of the trajectories of robot R_1 when outlier disturbances occur. The position errors of three mobile robots' trajectory estimations are shown in Fig. 4, where the blue ones are the filtering errors using EKF and the red ones are the filtering errors using REHF. It can be seen clearly from the simulation results that REHF performs better than EKF, which demonstrates that the REHF is more robust than EKF.

B. Experimental results of multi-robot cooperative localization on Pioneer3-DX robots

The proposed multi-robot cooperative localization approach has been implemented and tested in an indoor laboratory environment on two Pioneer3-DX mobile robots. For wireless communications, the robot is integrated with IEEE 802.11 based wireless network adapter allows wireless transparent TCP/IP using WaveLan. In our experiments, two mobile robots only use SICK LMS 200 laser range finder as sensor to perceive environment information. Mobile robots' odometry measurements come from wheel encoders. The velocities of robot R_1 and robot R_2 are all set to be 100mm/s . The sampling period of robot's odometer is 50ms and the multi-robot cooperative localization period is set to be $T = 0.5\text{s}$. It is noted that all parameters used in EKF and REHF are the same for all of the experiments with Pioneer3-DX. The choice of these parameters is determined according to the realistic characteristics of the robots and experimental scenes. Taking Q_{EKF} and Q_{REHF} for example, these parameters are determined by the hardware configuration of Pioneer3-DX and the encoder's characteristics installed in robot's wheels, which are $Q_{EKF} = Q_{REHF} = \text{diag}\{0.01^2, 0.01^2, 0.004^2, 0.01^2, 0.01^2, 0.004^2\}$. In EKF, R_{EKF} is updated according to covariance calculated in MbICP matching. In contrast to EKF, R_{REHF} is set as the same order of magnitude as R_{EKF} which is $R_{REHF} = \text{diag}\{0.004^2, 0.00174^2, 0.00174^2\}$. Moreover, γ is determined by a series of practical testing for parameter tuning and set to be $\gamma = 1$ in the REHF. The experimental scenes for our multi-robot cooperative localization system are shown in Fig. 5.

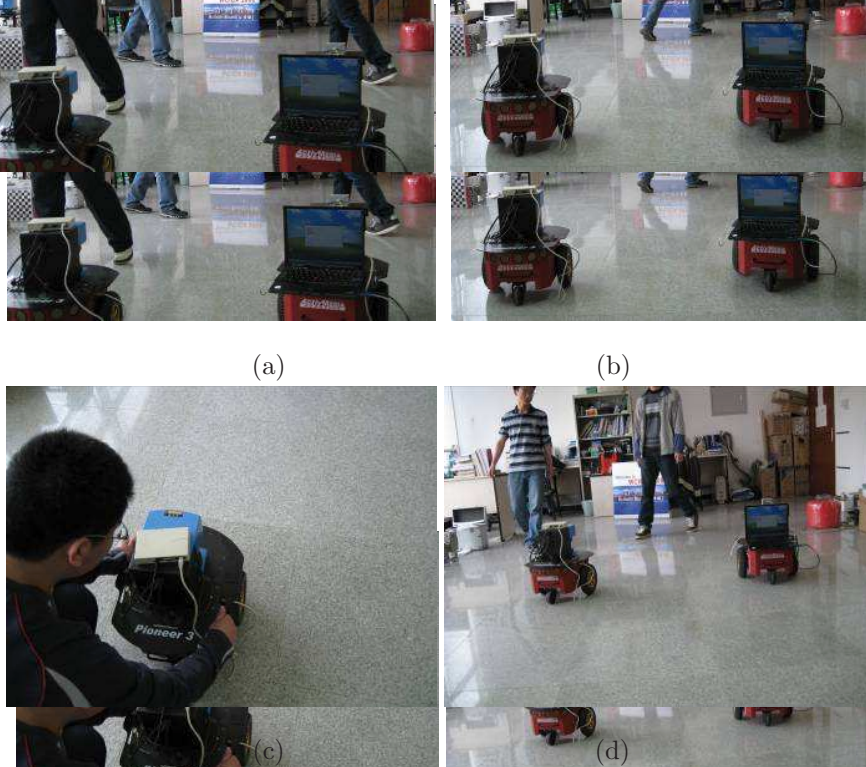


Fig. 5. The experimental scenes in the laboratory (about $8.8\text{m} \times 5.7\text{m}$). Some students were present in the front of two robots, which could be considered as dynamic obstacles. In order to simulate the unexpected collision in practical applications, robot R_1 in scene (c) was forced to rotate randomly for about 30° and lost its pose without being told.

In practical applications, mobile robot should have the ability to tackle typical non-Gaussian noises (unexpected collisions with passersby or other dynamic obstacles) with a better localization performance. During navigation, robots obtain and transmit the laser scanning data in real time. Two mobile robots' trajectories and the corresponding laser scanning data using dead reckoning, EKF and REHF are depicted in Fig. 6-8. An estimation of relative pose (position and orientation), i.e. $\hat{z}_{1,k} - \hat{z}_{2,k}$, is obtained in each localization period, and the laser scanning data of R_1 is transformed to the coordinate of R_2 by using the relative pose. Since these two mobile robots are working in the same scene, the laser scanning data of robot R_1 and robot R_2 should match perfectly if an accurately cooperative localization is implemented. However, filtering errors give rise to corresponding deviation in the estimation of relative pose, which can also be represented in the distribution of laser scanning data. In the experiment, robot R_1 was forced to rotate randomly for about 30° and lost its pose without being told (see Fig. 5(c)). If a better filtering performance is demonstrated in the experiment, a better convergence of the common areas composed of overlapping laser scanning data should be shown in Fig. 6-8 (data of R_1 and R_2 are depicted in red and blue points, respectively). As shown in Fig. 6, the laser scanning data of these two robots are dramatically separated because only dead reckoning is used. While a filtering algorithm is utilized in cooperative localization, the separation of laser scanning data can be overcome. Compared the experiment result in Fig. 7 with the one in Fig. 8, it can be seen clearly that REHF shows a superior performance than EKF.

In order to demonstrate and compare the effects of dead reckoning, EKF and REHF in the experiment, a bulletin board was arranged in the front of the experimental scene as a reference benchmark. The laser scanning data associated with this bulletin board is extracted, then least square line fitting algorithm is used

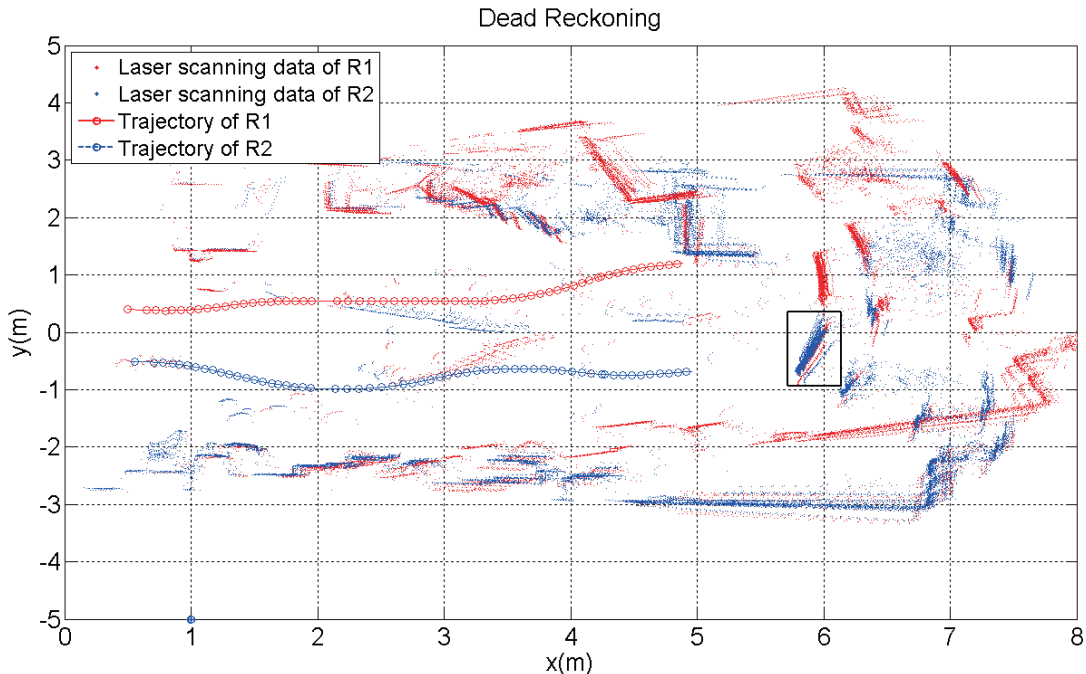


Fig. 6. Two robots' trajectories and the corresponding laser scanning data using dead reckoning in the laboratory scene.

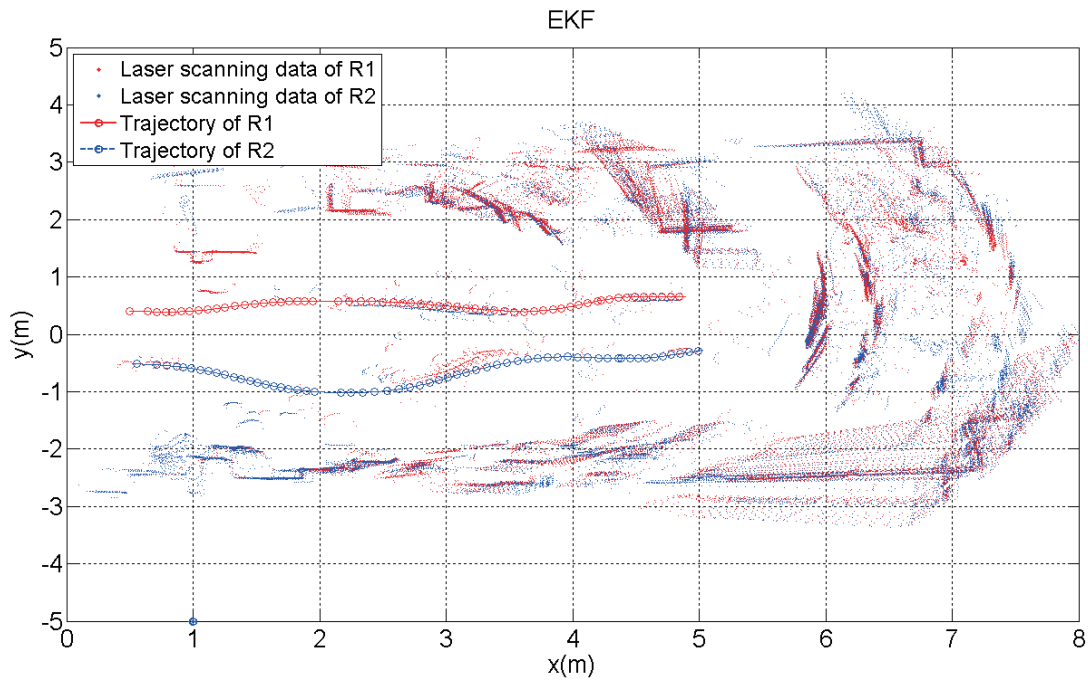


Fig. 7. Two robots' trajectories and the corresponding laser scanning data using EKF in the laboratory scene.

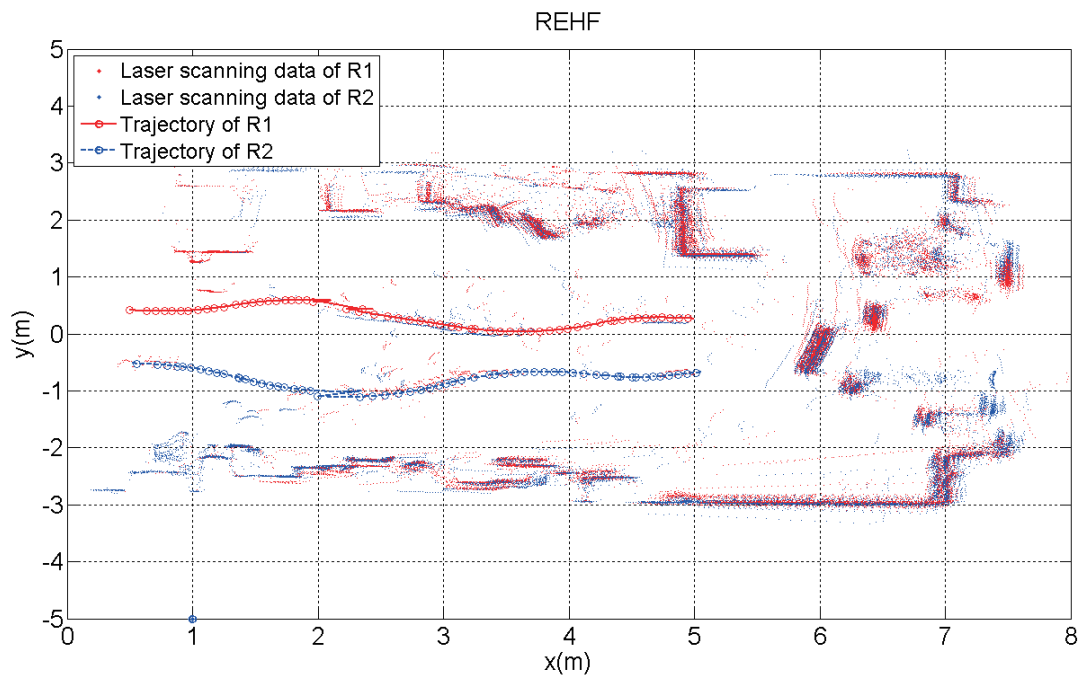


Fig. 8. Two robots' trajectories and the corresponding laser scanning data using REHF in the laboratory scene.

to estimate the reference benchmark in every localization period. As shown in Fig. 9, the numbers and distributions of the extracted scanning points in different localization period are not the same due to the different scanning distance and field of view, so the scanning data must be fitted in each localization period (depicted by blue lines one by one). The mean of the slope and intercept obtained in each line fitting is used to represent the final result of line fitting, which is defined as the reference line (depicted by the bold black

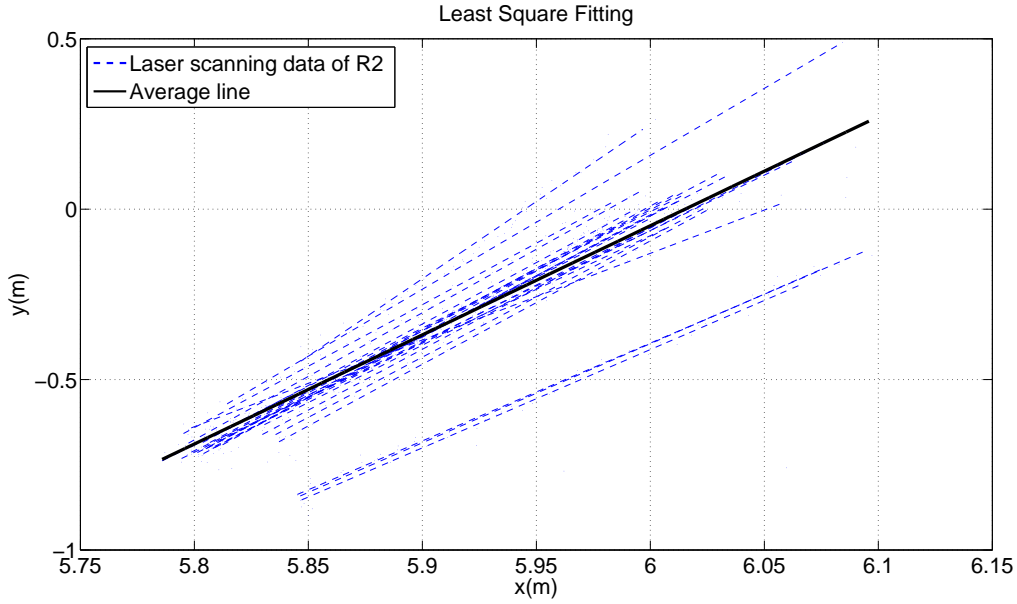


Fig. 9. The result of least square line fitting for laser scanning data associated with the bulletin board, which is marked by rectangular area in Fig. 6

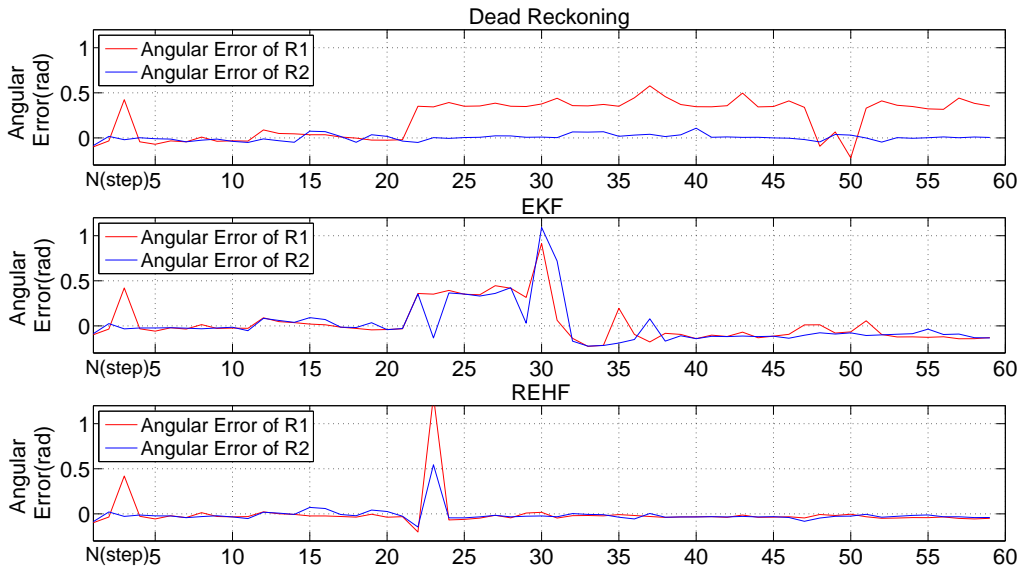


Fig. 10. The distribution of angular errors between each fitted line and the reference line in benchmark test using dead reckoning, EKF and REHF.

line in Fig. 9) in benchmark test.

In the experiment, robot R_2 was running stably and the noises in its odometer can be supposed as Gaussian. Furthermore, the trajectory of R_2 in Fig. 6 is estimated only using dead reckoning, so the corresponding laser scanning data of R_2 is not affected by the filtering algorithm of multi-robot cooperative localization. Therefore, the final result of line fitting of robot R_2 by using dead reckoning (see Fig. 9) is the best candidate taken as

the reference line. In order to compare the performance of EKF and REHF systematically and intensively, the laser scanning data (obtained by both R_1 and R_2) associated with the bulletin board are extracted and fitted in each localization period, and the distribution of angular errors between each fitted line and the reference line are depicted in Fig. 10. As shown in upper figure in Fig. 10, there is an obvious increase in angular errors of robots R_1 after step 21 due to the unexpected collision of R_1 in the experiment. When EKF is used in cooperative localization, angular errors of both two robots will change dramatically during step 21-40. However, when REHF is used in cooperative localization, angular errors of both two robots will change dramatically only during step 21-24, which shows that REHF yields better convergence rates than EKF in cooperative localization. Moreover, it can be seen clearly from the middle and lower figures in Fig. 10 that, as expected, angular errors in REHF are closer to zero than angular errors in EKF after step 40, which shows that REHF yields much better localization performance than EKF.

A group of experimental results of multi-robot cooperative localization in corridor scenes are given in Fig. 11-12. In the course of cooperative localization, a student in the corridor designedly made a collision with robot R_1 (the upper one with red trajectory) and robot R_1 was forced to rotate randomly to a certian extent. As shown in Fig. 11, there are still significant residual errors in the laser scanning data using EKF algorithm, which are caused by the collision happened in the experiment. Since EKF is not able to solve typical non-Gaussian noises such as unexpected collisions, these significant residual errors cannot be corrected successfully by using EKF. The main contribution in this paper is to propose the REHF algorithm to accomplish a better localization performance in dynamic environment. Compared with the laser scanning data matching result in Fig. 11, the matching result using REHF algorithm shows much less residual errors in Fig. 12.

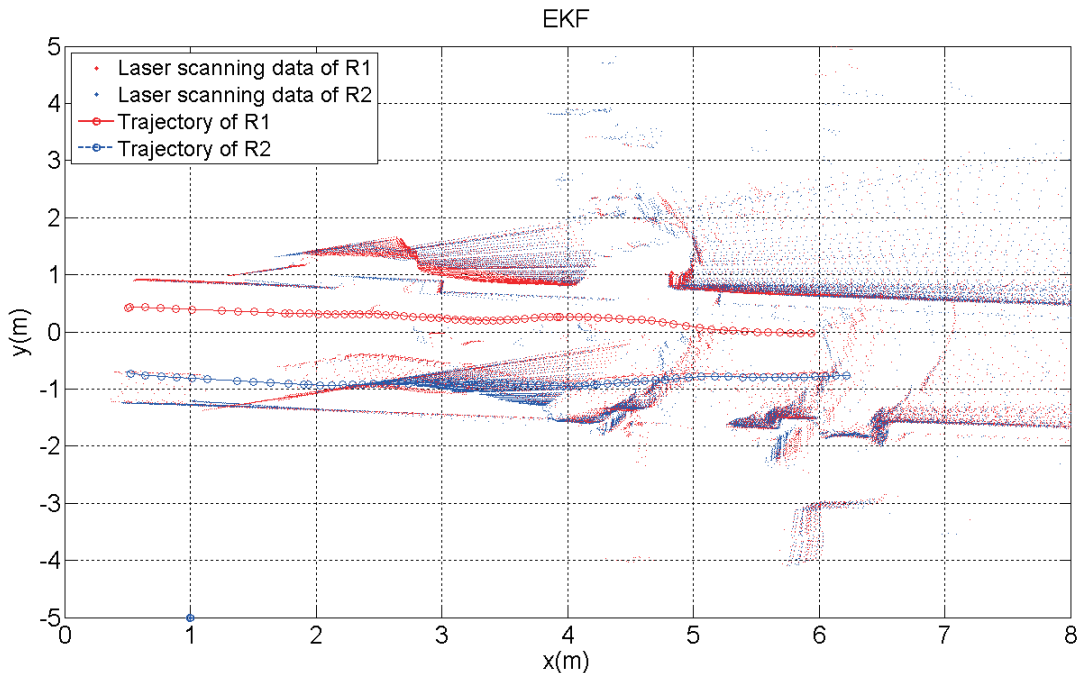


Fig. 11. Two mobile robots' trajectories and the corresponding laser scanning data using EKF in a corridor scene.

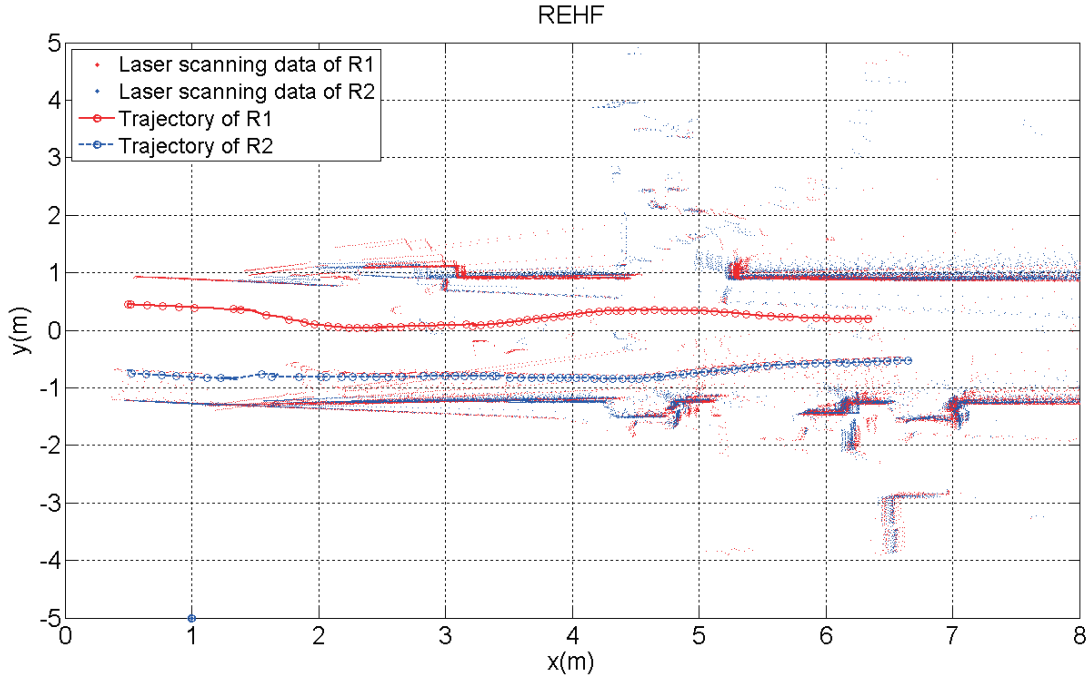


Fig. 12. Two mobile robots' trajectories and the corresponding laser scanning data using REHF in a corridor scene.

VI. CONCLUSION AND FUTURE WORK

This paper has focused on how to accomplish multi-robot cooperative localization using REHF and real-time laser data interaction. Compared with conventional multi-robot relative observations techniques, the MbICP-based 2D laser data matching algorithm could provide relative observations more accurately and conveniently, even in dynamic or semi-structured indoor environment. Since EKF relies on Gaussian approximations, there are considerable implementation difficulties in robotics applications when the system is highly nonlinear. In this work, the REHF algorithm has been proposed to accomplish a better multi-robot cooperative localization performance, which is shown to be robust against the dynamic disturbances in an unknown environment. Our future work will further test and improve the practicability of this approach in large-scale unstructured scenes and/or network-induced phenomena such as random sensor delays and sensor output missing (*Shen, Wang, Shu, & Wei 2009, Wei, Wang, & Shu 2009* and *Yang, Wang, Feng, & Liu 2009*).

REFERENCES

- Besl, P., & McKay, N. (1992). A method for registration of 3-d shapes, *IEEE Transactions on Pattern Analysis and Machine Intelligence*, 14(2), 239-256.
- Chen, H., Sun, D., Yang, J., & Chen, J. (2010). Localization for multirobot formations in indoor environment, *IEEE/ASME Transactions on Mechatronics*, 15(4), 561-574.
- Fox, D., Burgard, W., Kruppa, H., & Thrun, S. (2000). A probabilistic approach to collaborative multi-robot localization. *Autonomous Robots*, 8, 325-344.
- Hassibi, B., Sayed, A. H., & Kailath, T. (1999) *Indefinite quadratic estimation and control: a unified*

approach to H_2 and H_∞ theories. Philadelphia, PA: SIAM.

Howard, A., Mataric, M. J., & Sukhatme, G. S. (2002). Localization for mobile robot teams using maximum likelihood estimation, In *Proceedings of International Conference on Intelligent Robot and Systems*, Lausanne, Sept.

Huang, J., Farritor, S., Qadi, A., & Goddard, S. (2006). Localization and follow-the-leader control of a heterogeneous group of mobile robots, *IEEE/ASME Transactions on Mechatronics*, 11(2), 205-215.

Kondaxakis, P., Ruiz, V. F., & Harwin, W. S. (2004). Compensation of observability problem in a multi-robot localization scenario using CEKF, In *Proceedings of International Conference on Intelligent Robots and Systems*, Sendai, Sept.

Martinelli, A., Pont, F., & Siegwart, R. (2005). Multi-robot localization using relative observations, In *Proceedings of IEEE International Conference on Robotics and Automation*, Barcellona, April.

Minguez, J., Montesano, L., & Lamiroux, F. (2006). Metric-based iterative closest point scan matching for sensor displacement estimation, *IEEE Transactions on Robotics*, 22(5), 1047-1054.

Mourikis, A. I., & Roumeliotis, S. I. (2006a). Optimal sensor scheduling for resource-constrained localization of mobile robot formations. *IEEE Transactions on Robotics*, 22, 917-931.

Mourikis, A. I., & Roumeliotis, S. I. (2006b). Performance analysis of multirobot cooperative localization. *IEEE Transactions on Robotics*, 22, 666-681.

Nowzari, C., & Cortes, J. (2012). Self-triggered coordination of robotic networks for optimal deployment. *Automatica*, 48, 1077-1087.

Rekleitis, I. M., Dudek, G., & Milios, E. (2002). Multi-robot cooperative localization: a study of trade-off between efficiency and accuracy, In *Proceedings of International Conference on Intelligent Robot and Systems*, Lausanne, Sept.

Roumeliotis, S. I., & Bekey, G. A. (2002). Distributed multirobot localization, *IEEE Transactions on Robotics and Automation*, 18(5), 781-795.

Rooker, N., & Birk, A. (2007). Multi-robot exploration under the constraints of wireless networking. *Control Engineering Practice*, 14, 435-445.

Shen, B., Wang, Z., Shu, H., & Wei G. (2009). H_∞ filtering for nonlinear discrete-time stochastic systems with randomly varying sensor delays, *Automatica*, 45, 1032-1037.

Wei, G., Wang, Z., & Shu, H. (2009) Robust filtering with stochastic nonlinearities and multiple missing measurements, *Automatica*, 45, 836-841.

Yang, F., Wang, Z., Feng, G., & Liu, X. (2009). Robust filtering with randomly varying sensor delay: the finite-horizon case, *IEEE Transactions on Circuits and Systems - Part I*, 56(3), 664-672.

APPENDIX

The proof of Theorem 1

Before the proof of Theorem 1, we provide the following lemma.

Lemma 1 (Krein Space Kalman filter (*Hassibi, Sayed, & Kailath 1999*)) Given a Krein space discrete-time system:

$$x_{k+1} = A_k x_k + B_k w_k \quad (22)$$

$$y_k = C_k x_k + v_k \quad (23)$$

with the Gramian matrix

$$\left\langle \begin{bmatrix} x_0 \\ w_j \\ v_j \end{bmatrix}, \begin{bmatrix} x_0 \\ w_k \\ v_k \end{bmatrix} \right\rangle = \begin{bmatrix} P_{0|-1} & 0 & 0 \\ 0 & Q_k \delta_{jk} & 0 \\ 0 & 0 & R_k \delta_{jk} \end{bmatrix}, \quad (24)$$

both of which can be obtained from Krein space mapping corresponding to the indefinite quadratic function:

$$J = \|x_0 - \hat{x}_{0|-1}\|_{P_{0|-1}^{-1}}^2 + \sum_{k=0}^{N-1} \|w_k\|_{Q_k^{-1}}^2 + \sum_{k=0}^N \|(y_k - C_k x_k)\|_{R_k^{-1}}^2 \quad (25)$$

if $P_{0|-1} > 0$, $Q_k > 0$, R_k is invertible, and $\begin{bmatrix} A_k & B_k \end{bmatrix}$ has full rank for all k , the existence condition for the Krein space Kalman filter is given by:

$$P_{k|k}^{-1} = P_{k|k-1}^{-1} + C_k^T R_k^{-1} C_k > 0 \quad (26)$$

In addition, if this existence condition is satisfied, then the Krein space Kalman filtering equations is governed by:

Measurement update:

$$\hat{x}_{k|k} = \hat{x}_{k|k-1} + K_k (y_k - C_k \hat{x}_{k|k-1}) \quad (27)$$

$$P_{k|k} = P_{k|k-1} - P_{k|k-1} C_k^T (C_k P_{k|k-1} C_k^T + R_k)^{-1} C_k P_{k|k-1} \quad (28)$$

where the gain matrix K_k is defined by:

$$K_k = P_{k|k-1} C_k^T (C_k P_{k|k-1} C_k^T + R_k)^{-1} \quad (29)$$

Time update:

$$\hat{x}_{k+1|k} = A_k \hat{x}_{k|k} \quad (30)$$

$$P_{k+1|k} = A_k P_{k|k} A_k^T + B_k Q_k B_k^T \quad (31)$$

and the minimum point of the indefinite quadratic function J is provided by:

$$\min J(x_0, w, y) = \sum_{k=0}^N \|e_k\|_{(C_k P_{k|k-1} C_k^T + R_k)^{-1}}^2 \quad (32)$$

where the innovations e_k are defined by: $e_k = y_k - \hat{y}_{k|k-1} = y_k - C_k \hat{x}_{k|k-1}$

Proof of Theorem 1: In order to apply the approach of Krein space Kalman filtering (Lemma 1) to the robust extended H_∞ filtering problem, we adopt a mapping from the Hilbert space to the Krein space to solve the deterministic minimization problem. In Krein space, the minimization problem of a quadratic function can be cast into the Krein space Kalman filtering problem. We now convert the H_∞ performance (15) into the form of (25). Define

$$\begin{aligned} J_\infty &= \|z_0 - \hat{z}_{0|-1}\|_{P_{0|-1}}^2 + \sum_{k=0}^{N-1} \|\bar{\xi}_k\|_{Q_k}^2 + \sum_{k=0}^N \|\bar{\eta}_k\|_{R_k}^2 - \gamma^{-2} \sum_{k=0}^N \|\tilde{z}_k\|^2 \\ &= \|z_0 - \hat{z}_{0|-1}\|_{P_{0|-1}}^2 + \sum_{k=0}^{N-1} \|\bar{\xi}_k\|_{Q_k}^2 + \sum_{k=0}^N \|m_k - C_k z_k\|_{R_k}^2 - \gamma^{-2} \sum_{k=0}^N \|z_k - \tilde{z}_{k|k}\|^2 \\ &= \|z_0 - \hat{z}_{0|-1}\|_{P_{0|-1}}^2 + \sum_{k=0}^{N-1} \|\bar{\xi}_k\|_{Q_k}^2 + \sum_{k=0}^N \|\tilde{m}_k - \tilde{C}_k z_k\|_{\tilde{R}_k}^2 \end{aligned}$$

where

$$\tilde{m}_k = \begin{bmatrix} m_k \\ \hat{z}_{k|k} \end{bmatrix}, \quad \tilde{C}_k = \begin{bmatrix} C_k \\ I \end{bmatrix}, \quad \tilde{R}_k = \begin{bmatrix} R_k & 0 \\ 0 & -\gamma^2 I \end{bmatrix}. \quad (33)$$

Denote $\tilde{\eta}_k := \tilde{m}_k - \tilde{C}_k z_k$. Then, by Lemma 1, we can introduce the following Krein space system:

$$z_{k+1} = A_k z_k + \bar{\xi}_k \quad (34)$$

$$\tilde{m}_k = \tilde{C}_k z_k + \tilde{\eta}_k \quad (35)$$

with the Gramian matrix

$$\left\langle \begin{bmatrix} z_0 \\ \bar{\xi}_j \\ \tilde{\eta}_j \end{bmatrix}, \begin{bmatrix} z_0 \\ \bar{\xi}_k \\ \tilde{\eta}_k \end{bmatrix} \right\rangle = \begin{bmatrix} P_{0|-1} & 0 & 0 \\ 0 & Q_k \delta_{jk} & 0 \\ 0 & 0 & \tilde{R}_k \delta_{jk} \end{bmatrix}, \quad (36)$$

Now we are in a position to apply Lemma 1 to the robust extended H_∞ filtering problem. Note that there exist the following correspondences between the weighting matrixes in the cost function (25) of the Kalman filtering and those of the robust extended H_∞ filtering in (33): $Q_k \mapsto Q_k$, $R_k \mapsto \tilde{R}_k$.

In addition the following correspondences also exist between the system matrices of the Kalman filtering and those of the robust extended H_∞ filtering: $A_k \mapsto A_k$, $B_k \mapsto I$, $C_k \mapsto \tilde{C}_k$.

From the above correspondences, we can check that

$$\begin{aligned} P_{k|k}^{-1} &= P_{k|k-1}^{-1} + \tilde{C}_k^T \tilde{R}_k^{-1} \tilde{C}_k \\ &= P_{k|k-1}^{-1} + C_k^T R_k^{-1} C_k - \gamma^{-2} I, \end{aligned} \quad (37)$$

which is identical to (16). On the other hand, by using Lemma 1, we have

$$\begin{aligned}
\hat{z}_{k|k} &= \hat{z}_{k|k-1} + P_{k|k-1} \tilde{C}_k^T (\tilde{C}_k P_{k|k-1} \tilde{C}_k^T + \tilde{R}_k)^{-1} (\tilde{m}_k - \tilde{C}_k \hat{z}_{k|k-1}) \\
&= \hat{z}_{k|k-1} + P_{k|k-1} \begin{bmatrix} C_k^T & I \end{bmatrix} \\
&\quad \times \begin{bmatrix} I & -\hat{R}_k^{-1} C_k P_{k|k-1} \\ 0 & I \end{bmatrix} \\
&\quad \times \begin{bmatrix} \hat{R}_k & 0 \\ 0 & -\gamma^{-2} I + (P_{k|k-1}^{-1} + C_k^T C_k)^{-1} \end{bmatrix}^{-1} \\
&\quad \times \begin{bmatrix} I & 0 \\ -P_{k|k-1} C_k^T \hat{R}_k^{-1} & I \end{bmatrix} \\
&\quad \times \begin{bmatrix} m_k - C_k \hat{z}_{k|k-1} \\ \hat{z}_{k|k} - \hat{z}_{k|k-1} \end{bmatrix}
\end{aligned} \tag{38}$$

$$\tag{39}$$

where

$$\hat{R}_k = R_k + C_k P_{k|k-1} C_k^T. \tag{40}$$

By tedious but direct matrix inverse manipulation, we get

$$\hat{z}_{k|k} = \hat{z}_{k|k-1} + P_{k|k-1} C_k^T \hat{R}_k^{-1} (m_k - C_k \hat{z}_{k|k-1}) \tag{41}$$

which is same as (17). This completes the proof.